INTERNATIONAL JOURNAL FOR NUMERICAL METHODS IN FLUIDS
Int. J. Numer. Meth. Fluids 2010; **63**:1328–1346
Published online 5 August 2009 in Wiley InterScience (www.interscience.wiley.com). DOI: 10.1002/fld.2142

On the development of a triple-preserving Maxwell's equations solver in non-staggered grids

Tony W. H. Sheu[1, 2, 3, *, †], Y. W. Hung[1], M. H. Tsai[1], P. H. Chiu[1] and J. H. Li[1]

[1]*Department of Engineering Science and Ocean Engineering, National Taiwan University, No. 1, Sec. 4, Roosevelt Road, Taipei, Taiwan*
[2]*Taida Institute of Mathematical Science (TIMS), National Taiwan University, Taiwan*
[3]*Center for Quantum Science and Engineering (CQSE), National Taiwan University, Taiwan*

SUMMARY

We present in this paper a finite difference solver for Maxwell's equations in non-staggered grids. The scheme formulated in time domain theoretically preserves the properties of zero-divergence, symplecticity, and dispersion relation. The mathematically inherent Hamiltonian can be also retained all the time. Moreover, both spatial and temporal terms are approximated to yield the equal fourth-order spatial and temporal accuracies. Through the computational exercises, modified equation analysis and Fourier analysis, it can be clearly demonstrated that the proposed triple-preserving solver is computationally accurate and efficient for use to predict the Maxwell's solutions. Copyright © 2009 John Wiley & Sons, Ltd.

Received 13 October 2008; Revised 22 May 2009; Accepted 20 June 2009

KEY WORDS: Maxwell's equations; non-staggered grids; zero-divergence; symplecticity; dispersion relation; fourth order; triple-preserving solver

1. INTRODUCTION

The simulation of some differential equations of scientific and practical importance is subject to the divergence-free constraint conditions. One typical example of which is the incompressible Navier–Stokes equations, which should be solved together with the divergence-free velocity field $\underline{u}$. Unlike the incompressible Navier–Stokes equations, where $\nabla \cdot \underline{u} = 0$ serves as an explicit part of the equations of motion for the fluid flows, magnetohydrodynamic (MHD) and Maxwell's equations automatically satisfy the divergence-free conditions for the magnetic and electric flux densities

*Correspondence to: Tony W. H. Sheu, Department of Engineering Science and Ocean Engineering, National Taiwan University, No. 1, Sec. 4, Roosevelt Road, Taipei, Taiwan.
†E-mail: twhsheu@ntu.edu.tw

Contract/grant sponsor: National Science Council of the Republic of China; contract/grant numbers: NSC96-2221-E-002-293-MY2, NSC96-2221-E-002-004, CQSE97R0066-69

provided that their initial conditions are divergence free [1]. The presence of these two constraint equations cast in the divergence-free form poses a computational challenge since the numerically predicted solutions are not necessarily to be divergence free. Violation of these physically relevant divergence-free conditions can very often lead to severe numerical defects in stability.

Several numerical methods have been proposed to resolve the problems related to the local divergence-free conditions. For the incompressible Navier–Stokes equations, one may refer to the work of Karakashian and Jureidni [2]. In MHD equations, three major approaches have been proposed to overcome the difficulty associated with the predicted solutions that do not satisfy the divergence-free condition exactly or very accurately. They are known as the projection method of Brackbill and Barnes [3], constrained transport method of Evans and Hawley [4], and Powell's method [5], among many others reported in [6, 7]. To enforce the divergence-free conditions in Maxwell's equations, one can follow the idea of Yee [8] implemented in staggered grids. Another class of numerical methods for Maxwell's equations developed to retain the divergence-free condition is the generalized Lagrange multiplier formulation of Munz *et al.* [9]. The local divergence-free condition in Maxwell's equations can be also enforced within the discontinuous Galerkin framework [1].

Maxwell's equations have been gradually solved in time domain rather than in frequency domain since recent applications in semiconductor manufacturing, biophotonics, display technology, and optical communication, sensing, imaging and storage involve electromagnetic wave operated in high-frequency range. Development of an effective and accurate Maxwell's equation solver in time domain becomes thus an important subject. In Maxwell's equations, there are no magnetic and electric monopoles in the sense that the magnetic flux density $\underline{B}$ and electric flux density $\underline{D}$ satisfy the divergence-free constraint conditions given by $\nabla \cdot \underline{B} = 0$ and $\nabla \cdot \underline{D} = 0$. In the continuous context, these two divergence constraints have to be imposed initially. In fact, the divergence-free properties of $\underline{B}$ and $\underline{D}$ are preserved all the time by means of the time-evolving Faraday's and Ampère's laws. The implication is that the zero-divergence equations for $\underline{B}$ and $\underline{D}$ are considered as the inherent analytical properties for the evolution operators of the magnetic and electric fields. In other words, Gauss' law for magnetism and electricity can be left out of consideration in the analytic calculation of solutions for $\underline{B}$ and $\underline{D}$ from Faraday's and Ampère's laws, respectively.

In the discrete context of Maxwell's equations, the divergence-free conditions for magnetism and electricity are not satisfied in general due to the inevitably introduced discretization errors. Violation of the zero-divergence constraints on the magnetic and electric flux densities will often lead to stability problem in the simulation of Maxwell's equations. Thus, one major task needs to be performed in the development of numerical methods for Maxwell's equations is the elimination of divergence errors. Control of the divergence errors is particularly essential for solving the problem of compressible MHD, and the problem of Maxwell's equations, which may involve sharp gradient solutions, since any accumulated divergence error can cause the employed scheme to breakdown [10].

When approximating the derivative terms, numerical error will be inevitably shown both in amplitude and phase. The resulting dissipation error may attenuate the solution amplitude and the dispersion error may lead to an erroneously predicted phase speed. Maxwell's equations involve only the spatial terms of the first-order derivative type. Prediction error of the dispersive type can even cause the scheme destabilization to occur. It is therefore essential to avoid dispersion error when approximating the spatial derivative terms. How to preserve the embedded dispersion relation in the first-order derivative term becomes the second challenge of calculating an accurate Maxwell's solution.

DOI: 10.1002/fld

Dissipation error, which can result in amplitude attenuation, and dispersion error, which can cause an incorrect wave propagation speed, are cumulative in nature. After the wave being propagated for a fairly long distance or time, the solution for a time-evolving problem can be greatly affected and becomes non-physical. For example, the Hamiltonian structure of the Maxwell's equations may no longer be retained after a sufficiently long time. Preservation of the symplecticity embedded in Maxwell's equations poses another difficulty when approximating the time derivative terms shown in Faraday's and Ampère's equations.

The remainder of this paper will be organized as follows. In Section 2, Maxwell's equations, which include Faraday's law for the time-evolving magnetic flux density, Ampère's law for the time-evolving electric flux density, and Gauss' laws for magnetism and electricity, will be presented together with the physically important property of the zero-divergence for the two invoked vector fields. The hyperbolic Hamiltonian differential system will be integrated in time to preserve its symplecticity using the implicit symplectic Runge–Kutta scheme described in Section 3. This is followed by imposing the divergence-free algorithm for Gauss' law in Section 4 and presenting the discretization scheme in Section 5 for the first-order spatial derivative terms shown in the Maxwell's equations so as to preserve their respective dispersion relations. We present in Section 6 a detailed analysis of the scheme in Fourier space to reveal the accuracy of the proposed scheme. In Section 7, one problem with the analytic and benchmark solution will be chosen to validate the proposed fourth-order accurate scheme in time as well as in space, which accommodates the divergence-preserving, symplecticity-preserving and dispersion-relation-preserving properties. Finally, we will draw some conclusions in Section 8 based on the solutions predicted from the Maxwell's equations.

2. WORKING EQUATIONS

We consider in this paper the following time domain Maxwell's equations without current density and free charges for ease of describing the proposed scheme:

$$\frac{\partial \underline{H}}{\partial t} = -\frac{1}{\mu}\nabla \times \underline{E} \tag{1}$$

$$\frac{\partial \underline{E}}{\partial t} = \frac{1}{\varepsilon}\nabla \times \underline{H} \tag{2}$$

The above set of hyperbolic equations, which contain no current density, will be solved in a perfectly conducting domain bounded by some truncated boundaries, at which the following boundary conditions are specified:

$$\underline{n} \times \underline{E} = 0 \tag{3}$$

$$\underline{n} \cdot \underline{H} = 0 \tag{4}$$

In the above, $\underline{n}$ represents the unit vector that is locally orthogonal to a boundary surface. Imposition of the above set of boundary conditions ensures that the normal component of the magnetic field and the tangential component of the electric field will be vanished [11]. For the two-dimensional analysis, Maxwell's equations can be normally decomposed into two independent classes of equations, namely the transverse magnetic (TM) and the transverse electric (TE) modes. For brevity, only the TM-mode Maxwell's equations will be considered in this study.

DOI: 10.1002/fld

The permeability in Faraday's law of induction and the permittivity in Ampère's law for the medium of current interest are assumed to be homogeneous and isotropic for the sake of simplicity. These two material properties are the proportional constants for the following linear isotropic constitutive relations:

$$\underline{D} = \varepsilon \underline{E} \tag{5}$$

$$\underline{B} = \mu \underline{H} \tag{6}$$

The magnitudes of ε (dielectric permittivity) and μ (magnetic permeability) can, in addition, determine the wave speed $c(\equiv(\varepsilon\mu)^{1/2})$. In the above, four invoked field vectors $\underline{H}$, $\underline{E}$, $\underline{B}$, and $\underline{D}$ are denoted as the magnetic field intensity, electric field intensity, magnetic induction (or magnetic flux density), and electric displacement (or electric flux density), respectively. It is worth noticing here that the time-evolving transport equations for $\underline{H}$ and $\underline{E}$ are constrained by the following Gauss' laws for magnetism and electricity, respectively:

$$\nabla \cdot \underline{B} = 0 \tag{7}$$

$$\nabla \cdot \underline{D} = 0 \tag{8}$$

Within the continuous context, Equations (7)–(8) are satisfied automatically if they are divergence free initially [1]. Maxwell's equations (1)–(2) and (5)–(8) are, in mathematics, overdetermined. One often considers that the two divergence-free equations (7)–(8) are simply auxiliary and can be neglected when performing the numerical computations. The reason is that the equations in (1)–(2) are not strictly independent of (7)–(8) in the sense that Equations (7) and (8) turn out to be the direct consequence of applying the divergence operator $(\nabla\cdot)$ to both hand sides of Equations (1) and (2), respectively. One can therefore integrate the hyperbolic system of equations in (1)–(2) to calculate the instantaneous electric and magnetic fields. Negligence of the divergence-free equations (7)–(8) will destroy the ellipticity of Maxwell's equations in the spatial domain. In computational practice, satisfaction of two divergence-free constraint conditions shown in (7)–(8) poses however a great challenge due to the introduced numerical errors of all sorts. This misconception has been known to be the origin of the spurious solutions predicted in time domain [12, 13].

3. HAMILTONIAN STRUCTURE IN MAXWELL'S EQUATIONS

It is instructive to summarize some essential features existing in Maxwell's equations so that they can be taken into account in the scheme development. The hyperbolic system of equations (1)–(2) is equivalent to the dynamical system given below

$$\frac{\partial}{\partial t}\begin{pmatrix}\underline{H}\\ \underline{E}\end{pmatrix} = \begin{pmatrix}\underline{O} & -\underline{I}\\ \underline{I} & \underline{O}\end{pmatrix}\begin{pmatrix}\delta H/\delta \underline{E}\\ \delta H/\delta \underline{H}\end{pmatrix} \tag{9}$$

where $\delta H/\delta \underline{E}$, for example, denotes the variational (or functional) derivate of H with respect to $\underline{E}$. The Hamiltonian functional H shown above is expressed as follows [14]:

$$H(\underline{H}, \underline{E}) = \frac{1}{2}\int_\Omega \left(\frac{1}{\varepsilon}\underline{H}\cdot\nabla\times\underline{H} + \frac{1}{\mu}\underline{E}\cdot\nabla\times\underline{E}\right) \mathrm{d}\Omega \tag{10}$$

DOI: 10.1002/fld

According to the work of Kole *et al.* [15], Equations (1)–(2) can be rewritten as $(\partial/\partial t)\underline{\psi}(t) = \underline{\underline{G}}\,\underline{\psi}(t)$, where $\underline{\psi}(t) \equiv (\underline{m}, \underline{n}(t))^{\mathrm{T}}$ $(=\mu^{1/2}, \varepsilon^{1/2}\underline{E}(t))^{\mathrm{T}}$. The matrix operator $\underline{\underline{G}}$ given below is skew symmetric with respect to the inner product defined in [15]

$$\underline{\underline{G}} = \begin{pmatrix} O & -\mu^{-1/2}\nabla\times(\varepsilon^{-1/2}) \\ \varepsilon^{-1/2}\nabla\times(\mu^{-1/2}) & O \end{pmatrix} \tag{11}$$

Given Maxwell's equations represented by $\underline{\psi}(t)/\partial t = \underline{\underline{G}}\,\underline{\psi}(t)$, one can easily write its formal solution as $\underline{\psi}(t) = \mathrm{e}^{tG\psi(t=0)}$. It is then clear to us that Maxwell's equations under investigation will be evolved according to the mathematical operator given by $\mathrm{e}^{t\underline{\underline{G}}}$. It is also worth noticing that the norm of ψ, which is $\int_\Omega (\varepsilon\underline{E}\cdot\underline{E} + \mu\underline{H}\cdot\underline{H})\,\mathrm{d}\Omega$, has the direct relevance to the following energy density $W(t)$ for the EM mode of the field equations:

$$W(t) = \int_\Omega (\varepsilon\underline{E}\cdot\underline{E} + \mu\underline{H}\cdot\underline{H})\,\mathrm{d}\Omega \tag{12}$$

Owing to the time-evolving operator $\mathrm{e}^{t\underline{\underline{G}}}$, the vector solution for $\underline{\psi}(t)$ can be rotated without changing its magnitude [11]. This theoretically enlightened that the energy density given in (12) does not change with time for the EM field. Both of the local and global time-invariant quantities, defined, respectively, in (10) and (12), will be utilized later on as the indirect means to justify the proposed Maxwell's equations solver.

4. DIVERGENCE-FREE-PRESERVING SOLUTION ALGORITHM

There are six unknowns shown in Maxwell's equations (1)–(2) and (7)–(8), which include three equations (Faraday's law) for $\underline{B}$, three equations (Ampère's law) for $\underline{D}$, and two equations (Gauss' law) for magnetism and electricity. To close the differential system of Maxwell's equations, we normally only need to consider six of the eight equations given in (1) and (2), leaving the two elliptic equations (7) and (8) in Maxwell's equations out of consideration. Since omission of these divergence-free conditions may numerically result in a serious stability problem, we are motivated to develop a solution algorithm for Maxwell's equations so that the solutions predicted from (1)–(2) can satisfy Gauss' laws (7)–(8) all the time.

In the light that Gauss' laws shown in (7)–(8) are satisfied only within the continuous context through Equations (1) and (2) for the field vectors $\underline{H}$ and $\underline{E}$, modification of the time-evolving transport equations for them is needed for retaining the discrete divergence-free solutions. Inspired by the work of Assous *et al.* [16], two potential functions Φ_1 and Φ_2 will be introduced into Equations (2) and (1), respectively. It is hoped that analysis of the following Faraday's and Ampère's equations can ensure a discrete satisfaction of the normally dispensed Gauss' laws:

$$\frac{\partial}{\partial t}\underline{E} - \frac{1}{\varepsilon}\nabla\times\underline{H} + \nabla\Phi_1 = 0 \tag{13}$$

$$\frac{\partial}{\partial t}\underline{H} + \frac{1}{\mu}\nabla\times\underline{E} + \nabla\Phi_2 = 0 \tag{14}$$

DOI: 10.1002/fld

To close the differential system for the above set of modified Maxwell's equations, two equations for the correction potentials Φ_1 and Φ_2 need to be derived. Define first the differential operators D_1 and D_2 for the Gauss' law represented by Equations (8) and (7), respectively. One can then write the modified Gauss' law as follows:

$$D_1\Phi_1+\nabla\cdot\underline{E}=0 \tag{15}$$

$$D_2\Phi_2+\nabla\cdot\underline{H}=0 \tag{16}$$

By performing the differential operator $(\nabla\cdot)$ on Equation (13) and then the temporal operator $\partial/\partial t$ on Equation (15), one can derive the equation for Φ_1 as follows:

$$\frac{\partial(D_1\Phi_1)}{\partial t}-\nabla^2\Phi_1=-\frac{1}{\varepsilon}\nabla\cdot(\nabla\times\underline{H}) \tag{17}$$

Since $D_1\Phi_1=-\nabla\cdot\underline{E}$, we are led to rewrite Equation (17) as

$$\nabla^2\Phi_1=-\frac{\partial}{\partial t}(\nabla\cdot\underline{E}) \tag{18}$$

For the two-dimensional case, the equation governing the correction function Φ_1 turns out to be the Laplace equation $\nabla^2\Phi_1=0$ due to the assumption that both current density and electric charge density are equal to zero.

For solving the value of Φ_1 from the Laplace equation, we need to prescribe the boundary condition. In this study, we impose $\partial\Phi_1/\partial x=0$ and $\partial\Phi_1/\partial y=0$ at the boundary since $\partial\underline{E}/\partial t-(1/\varepsilon)\nabla\times\underline{H}=(0,0)$ holds on the x–y plane. As a result, Φ_1 will remain to be zero in the whole domain and there is no need for us to include Equation (18) in the current two-dimensional simulation. One can similarly perform the spatial operator $(\nabla\cdot)$ on Equation (14) and the temporal differential operator $\partial/\partial t$ on Equation (16) to get the transport equation for Φ_2 as follows, thanks to the identity $\nabla\cdot(\nabla\times\underline{E})=0$

$$\nabla^2\Phi_2=-\frac{\partial}{\partial t}(\nabla\cdot\underline{H}) \tag{19}$$

In summary, the divergence-free electromagnetic differential system formulated within the above framework of Lagrange multiplier includes the equations given in (13), (14), (19) and $\Phi_1=0$.

5. DISCRETIZATION METHOD

We consider in this paper the following equations with the TM polarization to model the time-evolving planar magnetic field $(H_x, H_y, 0)$ and the scalar electric field $(0, 0, E_z)$

$$\frac{\partial H_x}{\partial t}=-\frac{1}{\mu}\frac{\partial E_z}{\partial y}-\frac{\partial\Phi_2}{\partial x}$$

$$\frac{\partial H_y}{\partial t}=\frac{1}{\mu}\frac{\partial E_z}{\partial x}-\frac{\partial\Phi_2}{\partial y}$$

DOI: 10.1002/fld

$$\begin{aligned}\frac{\partial E_z}{\partial t} &= \frac{1}{\varepsilon}\left(\frac{\partial H_y}{\partial x} - \frac{\partial H_x}{\partial y}\right)\\ \nabla^2\Phi_2 &= -\frac{\partial}{\partial t}\left(\frac{\partial H_x}{\partial x} + \frac{\partial H_y}{\partial y}\right)\end{aligned} \tag{20}$$

Maxwell's equations, which are utilized to describe the propagation of electromagnetic wave in space and time, have been shown to accommodate the Hamiltonian structure [17, 18]. It was shown in [19, 20] that symplectic schemes in theory outperform their non-symplectic counterparts since only the former schemes can always preserve the Hamiltonian nature embedded in Maxwell's equations.

5.1. Symplecticity-preserving temporal scheme

For retaining the physically embedded Hamiltonian structure in Maxwell's equations [17, 18], we will present below the employed symplectic integrator for the time derivative terms shown in Equation (20).

The first three equations in (20) can be written as $\partial\underline{\phi}/\partial t = \underline{f}$, where

$$\underline{\phi} = (H_x, H_y, E_z)^{\mathrm{T}} \tag{21}$$

$$\underline{f} = \left(-\frac{1}{\mu}\partial E_z/\partial y - \partial\Phi_2/\partial x, \frac{1}{\mu}\partial E_z/\partial x - \partial\Phi_2/\partial y, \frac{1}{\varepsilon}(\partial H_y/\partial x - \partial H_x/\partial y)\right)^{\mathrm{T}} \tag{22}$$

One of the representative scalar equations in $\partial\underline{\phi}/\partial t = \underline{f}$, which is given by

$$\partial\phi/\partial t = f \tag{23}$$

will be approximated within the semi-discretization framework. By applying the symplectic Runge–Kutta scheme of the fourth-order accuracy in time [10], we are rendered to get the following three equations which altogether permit the fourth-order temporal accuracy for Equation (23):

$$\phi^{(1)} = \phi^n + \Delta t[\tfrac{1}{4}f^{(1)} + (\tfrac{1}{4} + \tfrac{1}{2\sqrt{3}})f^{(2)}] \tag{24}$$

$$\phi^{(2)} = \phi^n + \Delta t[(\tfrac{1}{4} - \tfrac{1}{2\sqrt{3}})f^{(1)} + (\tfrac{1}{4})f^{(2)}] \tag{25}$$

$$\phi^{n+1} = \phi^n + \Delta t[\tfrac{1}{2}f^{(1)} + \tfrac{1}{2}f^{(2)}] \tag{26}$$

where $f^{(1)}$ and $f^{(2)}$ represent the values of f evaluate at $t = n + (\frac{1}{2} + \frac{1}{2\sqrt{3}})\,\mathrm{d}t$ and $t = n + (\frac{1}{2} - \frac{1}{2\sqrt{3}})\,\mathrm{d}t$, respectively.

5.2. Dispersion-relation-preserving explicit compact spatial scheme

Discretization of Maxwell's equations remains to approximate the first-order spatial derivative terms shown in Equation (22) to render the algebraic system for equations in (20). One should notice that when discretizing all the first-order derivative terms, shown in (20), in non-staggered grids, care needs to be properly taken of. Otherwise, undesirable numerical oscillations, which are

DOI: 10.1002/fld

Figure 1. Schematic of the seven-point stencil used in the current scheme.

commonly referred to as the numerical errors due to the even–odd or checkerboard decoupling, will be present.

In the approximation of $\partial H_x/\partial x$, for example, at a point (i, j), it is essential to take the nodal value of $H_x|_{i,j}$ into consideration so as to avoid the so-called even–odd decoupling problem. To enhance numerical stability, one can employ the compact scheme proposed earlier in [21, 22]. Referring to Figure 1, $\partial H_x/\partial x|_{i,j}$ will be approximated by the following equation in a mesh with the grid size of h:

$$\left.\frac{\partial H_x}{\partial x}\right|_{i,j} = a_1 H_x|_{i+3,j} + a_2 H_x|_{i+2,j} + a_3 H_x|_{i+1,j} - a_3 H_x|_{i-1,j} - a_2 H_x|_{i-2,j} - a_1 H_x|_{i-3,j} \tag{27}$$

Derivation of the compact scheme for $\partial H_x/\partial x$ is followed by applying the Taylor series expansion for $H_x|_{i\pm1,j}$, $H_x|_{i\pm2,j}$, and $H_x|_{i\pm3,j}$ with respect to $H_x|_{i,j}$ and, then, eliminating the two leading error terms $\partial^2 H_x/\partial x^2$ and $\partial^3 H_x/\partial x^3$ shown in the modified equation. One more algebraic equation needs to be derived for uniquely determining the three weighting coefficients a_1, a_2, and a_3 introduced in (27).

Within the dispersion relation preserving (DRP) analysis framework [23], we define first the Fourier transform and its inverse for $\partial H_x/\partial x$ in the one space dimension x as follows:

$$\tilde{H}_x(\alpha) = \frac{1}{2\pi}\int_{-\infty}^{+\infty} H_x(x)\ \mathrm{e}^{-\mathbf{i}\alpha x}\,\mathrm{d}x \tag{28}$$

$$H_x(x) = \int_{-\infty}^{+\infty} \tilde{H}_x(\alpha)\mathrm{e}^{\mathbf{i}\alpha x}\,\mathrm{d}\alpha \tag{29}$$

By conducting Fourier transform on each term shown in Equation (27), we are led to get the following actual wavenumber α:

$$\alpha \simeq \frac{-\mathbf{i}}{h}(a_1\mathrm{e}^{\mathbf{i}3\alpha h} + a_2\mathrm{e}^{\mathbf{i}2\alpha h} + a_3\ \mathrm{e}^{\mathbf{i}\alpha h} - a_3\ \mathrm{e}^{-\mathbf{i}\alpha h} - a_2\ \mathrm{e}^{-\mathbf{i}2\alpha h} - a_1\ \mathrm{e}^{-\mathbf{i}3\alpha h}) \tag{30}$$

In an approximation sense, the effective wavenumber $\tilde{\alpha}$ can be regarded as the right-hand side of Equation (41) [23]. In other words, we can define $\tilde{\alpha}$ as follows:

$$\tilde{\alpha} = \frac{-\mathbf{i}}{h}(a_1\mathrm{e}^{\mathbf{i}3\alpha h} + a_2\mathrm{e}^{\mathbf{i}2\alpha h} + a_3\mathrm{e}^{\mathbf{i}\alpha h} - a_3\mathrm{e}^{-\mathbf{i}\alpha h} - a_2\mathrm{e}^{-\mathbf{i}2\alpha h} - a_1\ \mathrm{e}^{-\mathbf{i}3\alpha h}) \tag{31}$$

where $\mathbf{i} = \sqrt{-1}$. To make $\tilde{\alpha}$ a good approximation of α, the magnitude of $|\alpha h - \tilde{\alpha}h|^2$ should be kept as small as possible in the integral range of $-\pi/2 \leqslant \gamma \leqslant \pi/2$

$$E(\alpha) = \int_{-\pi/2}^{\pi/2} |\alpha h - \tilde{\alpha}h|^2\,\mathrm{d}(\alpha h) = \int_{-\pi/2}^{\pi/2} |\gamma - \tilde{\gamma}|^2\,\mathrm{d}\gamma \tag{32}$$

DOI: 10.1002/fld

where $\gamma=\alpha h$. To make the positive E a minimum magnitude, the following equation is enforced to achieve the goal:

$$\frac{\partial E}{\partial a_3}=0 \tag{33}$$

According to the above extreme condition, we are led to derive one algebraic equation. One equation for the minimization of dispersion error will be used together with the other two equations derived from the modified equation analysis to get the following three coefficients a_i $(i=1\text{–}3)$ shown in Equation (27)

$$a_1=-\frac{2(3\pi-10)}{3(15\pi-32)} \tag{34}$$

$$a_2=\frac{3(9\pi-32)}{4(15\pi-32)} \tag{35}$$

$$a_3=\frac{12}{15\pi-32} \tag{36}$$

Thanks to the following modified equation for $\partial H_x/\partial x$, we are led to know that the proposed dispersion relation-preserving scheme has the spatial accuracy of fourth order

$$\frac{\partial H_x}{\partial x}=\frac{\partial H_x}{\partial x}\bigg|_{\text{exact}}-\frac{9(5\pi-16)}{10(15\pi-32)}h^4\frac{\partial^5 H_x}{\partial x^5}+O(h^6)+\cdots \tag{37}$$

While use of the above implicit compact scheme can circumvent the erroneously predicted oscillatory solutions, the computational cost can be quite considerable. As a means to alleviate this drawback but not at the cost of destabilizing the approximation, we employ in this study the modified explicit compact scheme presented in [24]. In what follows, we will briefly describe this scheme. In the seven-point solution stencil schematic in Figure 1, the implicit equation for $\partial H_x/\partial x$ can be written in matrix form given below for the vector field $\underline{\mathbf{H}_x}(\equiv(H_x|_1, H_x|_2, \ldots, H_x|_7)^{\mathrm{T}})$:

$$\underline{\underline{\mathbf{A}}}\,\underline{\mathbf{H}'_x}=\underline{\underline{\mathbf{B}}}\,\underline{\mathbf{H}_x} \tag{38}$$

where $\underline{\mathbf{H}'_x}\equiv\partial\underline{\mathbf{H}_x}/\partial x$ and

$$\underline{\underline{\mathbf{A}}}=\begin{bmatrix}
1 & 3 & & & & & \\
\frac{1}{4} & 1 & \frac{1}{4} & & & & \\
 & \frac{1}{4} & 1 & \frac{1}{4} & & & \\
 & & & 1 & & & \\
 & & & \frac{1}{4} & 1 & \frac{1}{4} & \\
 & & & & \frac{1}{4} & 1 & \frac{1}{4} \\
 & & & & & 3 & 1
\end{bmatrix}$$

DOI: 10.1002/fld

$$\underline{\underline{\mathbf{B}}}=\begin{bmatrix}
-\frac{17}{6} & \frac{3}{2} & \frac{3}{2} & -\frac{1}{6} & & & \\
-\frac{3}{4} & 0 & \frac{3}{4} & & & & \\
 & \frac{3}{4} & 0 & \frac{3}{4} & & & \\
\frac{2(-10+3\pi)}{3(-32+15\pi)} & -\frac{3(-32+9\pi)}{4(-32+15\pi)} & -\frac{12}{-32+15\pi} & 0 & \frac{12}{-32+15\pi} & \frac{3(-32+9\pi)}{4(-32+15\pi)} & -\frac{2(-10+3\pi)}{3(-32+15\pi)} \\
 & & & -\frac{3}{4} & 0 & \frac{3}{4} & \\
 & & & & -\frac{3}{4} & 0 & \frac{3}{4} \\
 & & & \frac{1}{6} & -\frac{3}{2} & -\frac{3}{2} & \frac{17}{6}
\end{bmatrix}$$

The gradient vector $\underline{\mathbf{H}}'_x(\equiv(\partial H_x/\partial x|_1, \partial H_x/\partial x|_2, \ldots, \partial H_x/\partial x|_7)^{\mathrm{T}})$ shown in Equation (38) can be also written as $\underline{\mathbf{H}}'_x=\underline{\underline{\mathbf{G}}}\,\underline{\mathbf{H}}_x$, where $\underline{\underline{\mathbf{G}}}(\equiv\underline{\underline{\mathbf{A}}}^{-1}\underline{\underline{\mathbf{B}}})$ is derived as

$$\underline{\underline{\mathbf{G}}}=\begin{bmatrix}
-\frac{-152+69\pi}{2(-32+15\pi)} & \frac{3(-224+99\pi)}{4(-32+15\pi)} & -\frac{3(-104+45\pi)}{2(-32+15\pi)} & \frac{13}{6} & -\frac{12}{-32+15\pi} & -\frac{3(-32+9\pi)}{4(-32+15\pi)} & \frac{2(-10+3\pi)}{3(-32+15\pi)} \\
-\frac{4(-11+6\pi)}{9(-32+15\pi)} & -\frac{160+69\pi}{4(-32+15\pi)} & \frac{2(-34+15\pi)}{-32+15\pi} & -\frac{7}{9} & \frac{4}{-32+15\pi} & \frac{-32+9\pi}{4(-32+15\pi)} & -\frac{2(-10+3\pi)}{9(-32+15\pi)} \\
\frac{8+3\pi}{18(-32+15\pi)} & -\frac{-32+21\pi}{4(-32+15\pi)} & -\frac{5(-8+3\pi)}{2(-32+15\pi)} & \frac{17}{18} & -\frac{4}{-32+15\pi} & -\frac{-32+9\pi}{4(-32+15\pi)} & \frac{2(-10+3\pi)}{9(-32+15\pi)} \\
\frac{2(-10+3\pi)}{3(-32+15\pi)} & -\frac{3(-32+9\pi)}{4(-32+15\pi)} & -\frac{12}{-32+15\pi} & 0 & \frac{12}{-32+15\pi} & \frac{3(-32+9\pi)}{4(-32+15\pi)} & -\frac{2(-10+3\pi)}{3(-32+15\pi)} \\
-\frac{2(-10+3\pi)}{9(-32+15\pi)} & \frac{-32+9\pi}{4(-32+15\pi)} & \frac{4}{-32+15\pi} & -\frac{17}{18} & \frac{5(-8+3\pi)}{2(-32+15\pi)} & \frac{-32+21\pi}{4(-32+15\pi)} & -\frac{8+3\pi}{18(-32+15\pi)} \\
\frac{2(-10+3\pi)}{9(-32+15\pi)} & -\frac{-32+9\pi}{4(-32+15\pi)} & -\frac{4}{-32+15\pi} & \frac{7}{9} & -\frac{2(-34+15\pi)}{-32+15\pi} & \frac{160+69\pi}{4(-32+15\pi)} & \frac{4(-11+6\pi)}{9(-32+15\pi)} \\
-\frac{2(-10+3\pi)}{3(-32+15\pi)} & \frac{3(-32+9\pi)}{4(-32+15\pi)} & \frac{12}{-32+15\pi} & -\frac{13}{6} & \frac{3(-104+45\pi)}{2(-32+15\pi)} & -\frac{3(-224+99\pi)}{4(-32+15\pi)} & \frac{-152+69\pi}{2(-32+15\pi)}
\end{bmatrix}$$

6. ANALYSIS OF THE PROPOSED SCHEME IN FOURIER SPACE

The following approximation for the first derivative of ϕ, which represents E_z, H_x, H_y, is considered in one dimension:

$$\left.\frac{\partial\phi}{\partial x}\right|_{i,j}=a_1\phi|_{i+3,j}+a_2\phi|_{i+2,j}+a_3\phi|_{i+1,j}-a_3\phi|_{i-1,j}-a_2\phi|_{i-2,j}-a_1\phi|_{i-3,j} \tag{39}$$

For the purpose of conducting Fourier analysis, field variable ϕ is assumed to be periodic over the domain $[0\sim L]$, i.e. $\phi_1=\phi_{N+1}$, where $N=L/h$ and h is the grid size. Within the Fourier analysis framework, ϕ can be decomposed into the Fourier series expansion shown below [25],

$$\phi(x)=\sum_{k=-N/2}^{k=N/2}\tilde{\phi}(k)\mathrm{e}^{\mathbf{i}2\pi kx/L} \tag{40}$$

DOI: 10.1002/fld

where $\mathbf{i}=\sqrt{-1}$. It is convenient to introduce a scaled wavenumber $\alpha=2\pi kh/L=2\pi k/N$, and a scaled coordinate $s=x/h$. The Fourier modes expressed in terms of these are simply $\exp(\mathbf{i}\alpha s)$. By conducting the above transform on each term shown in Equation (39), we are led to get the following actual wavenumber α:

$$\alpha\simeq\frac{-\mathbf{i}}{h}(a_1\mathrm{e}^{\mathbf{i}3\alpha h}+a_2\mathrm{e}^{\mathbf{i}2\alpha h}+a_3\mathrm{e}^{\mathbf{i}\alpha h}-a_3\mathrm{e}^{-\mathbf{i}\alpha h}-a_2\mathrm{e}^{-\mathbf{i}2\alpha h}-a_1\mathrm{e}^{-\mathbf{i}3\alpha h}) \tag{41}$$

In an approximation sense, the effective wavenumber $\tilde{\alpha}$ can be regarded as the right-hand side of Equation (41) [23]. In other words, we can define $\tilde{\alpha}$ as follows:

$$\tilde{\alpha}=\frac{-\mathbf{i}}{h}(a_1\mathrm{e}^{\mathbf{i}3\alpha h}+a_2\mathrm{e}^{\mathbf{i}2\alpha h}+a_3\mathrm{e}^{\mathbf{i}\alpha h}-a_3\mathrm{e}^{-\mathbf{i}\alpha h}-a_2\mathrm{e}^{-\mathbf{i}2\alpha h}-a_1\mathrm{e}^{-\mathbf{i}3\alpha h}) \tag{42}$$

It follows that:

$$\tilde{\alpha}h=-\mathbf{i}(a_1\mathrm{e}^{\mathbf{i}3\alpha h}+a_2\mathrm{e}^{\mathbf{i}2\alpha h}+a_3\mathrm{e}^{\mathbf{i}\alpha h}-a_3\mathrm{e}^{-\mathbf{i}\alpha h}-a_2\mathrm{e}^{-\mathbf{i}2\alpha h}-a_1\mathrm{e}^{-\mathbf{i}3\alpha h}) \tag{43}$$

Fundamental analysis of the present DRP scheme starts from defining the coefficients k_i and k_r for the respective dispersion and dissipation errors

$$k_i=\Re[\tilde{\alpha}h] \tag{44}$$

$$k_r=\Im[\tilde{\alpha}h] \tag{45}$$

In the above, $\Re[\tilde{\alpha}h]$ denotes the real part of $\tilde{\alpha}h$ and $\Im[\tilde{\alpha}h]$ stands for the imaginary part of $\tilde{\alpha}h$ for the proposed scheme. It is worth noticing that k_r is always zero for the present scheme due to the symmetry of the stencil points. In Figure 2, the predicted values of k_i are plotted against the modified wavenumber αh. For the sake of comparison, we also plot k_i for the scheme of Tam and Webb [23], schemes of Lele [25], and schemes of Bogey and Bailly [26].

7. NUMERICAL RESULTS

To demonstrate the integrity of the symplecticity-preserving scheme formulated in non-staggered grids for simulating the TM wave, we will consider the problem amenable to the analytic solutions. The two-dimensional problem will be solved at $\mu=1$ and $\varepsilon=1$ in $-1\leqslant x\leqslant 1$, $-1\leqslant y\leqslant 1$ with the initially prescribed divergence-free conditions for $\underline{H}$ and $\underline{E}$ as follows:

$$E_z(x,y,0)=\sin(3\pi x)\sin(4\pi y)$$

$$H_x(x,y,0)=-\tfrac{4}{5}\cos(3\pi x)\cos(4\pi y)$$

$$H_y(x,y,0)=-\tfrac{3}{5}\sin(3\pi x)\sin(4\pi y)$$

The corresponding exact solutions are given below [10]

$$E_z(x,y,t)=\sin(3\pi x-5\pi t)\sin(4\pi y)$$

$$H_x(x,y,t)=-\tfrac{4}{5}\cos(3\pi x-5\pi t)\cos(4\pi y)$$

$$H_y(x,y,t)=-\tfrac{3}{5}\sin(3\pi x-5\pi t)\sin(4\pi y)$$

DOI: 10.1002/fld

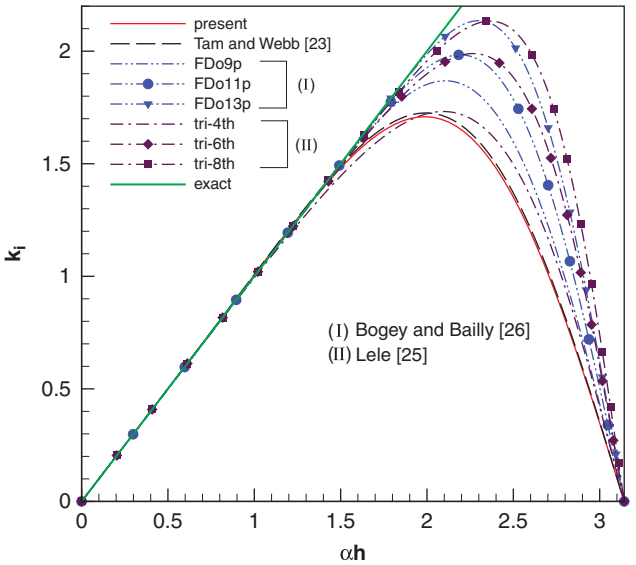

Figure 2. Comparison of the values of k_i, which are plotted against the modified wavenumber αh, among the proposed scheme (seven stencil points), the scheme of Tam and Webb (seven stencil points) [23], the schemes of Bogry and Bailly (nine-thirteen stencil points) [26], and the tri-diagonal compact schemes of Lele (seven stencil points) [25].

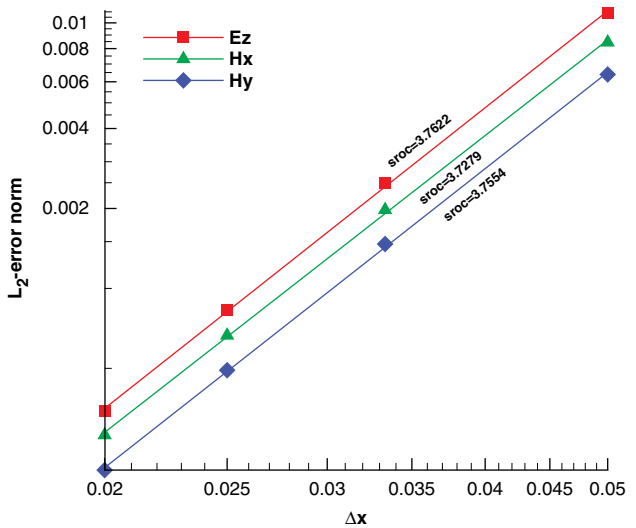

Figure 3. The predicted L_2-error norms and the corresponding spatial rates of convergence (sroc) for the three field variables.

Two sets of calculations will be performed to get the spatial and temporal rates of convergence. One set of calculations will be performed at $\Delta t = \frac{1}{5000}$, which is much smaller than the finest grids

DOI: 10.1002/fld

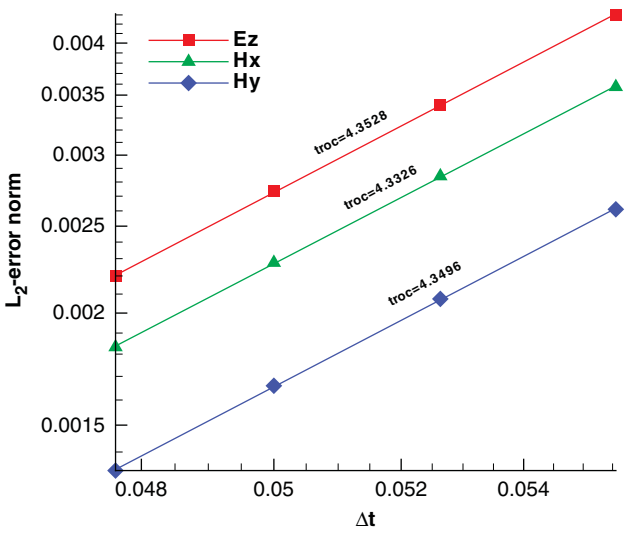

Figure 4. The predicted L_2-error norms and the corresponding temporal rates of convergence (troc) for the three field variables.

of $\Delta x = \Delta y = \frac{1}{20}, \frac{1}{30}, \frac{1}{40}, \frac{1}{50}$. The predicted errors cast in L_2-error norms are plotted in Figure 3, from which the spatial rate of convergence can be numerically predicted to be fourth. Another set of calculations will be similarly performed at the fixed grid size $\Delta x = \Delta y = \frac{1}{50}$, which is again much smaller than the smallest chosen time steps of $\Delta t = \frac{1}{18}, \frac{1}{19}, \frac{1}{20}, \frac{1}{21}$, to facilitate us to calculate the temporal rate of convergence. As Figure 4 shows, the L_2-error norms are decreased with the decreasing values of Δt at an approximated rate of fourth.

As an indirect justification of the proposed scheme, we will calculate the values for the Hamiltonian defined in (10) and the energy density given in (12). Note that the Hamiltonian is trivially equal to zero in the present two-dimensional Maxwell's equations. This implies that the Hamiltonian structure will be automatically preserved all the time for the TM wave problem. We need, as a result, to plot only the predicted and exact energy density W against time in Figure 5, from which one can clearly see that the currently predicted value of W does not vary with time. Based on the predicted solution, we will calculate the L_2-norms of $\nabla \cdot \underline{H}$ and then plot them against time. From Figure 6, one can clearly see that the magnetic field is indeed discretely divergence free for the calculation without taking the differential Gauss' law into account in the prediction.

To examine how the correction potential Φ_2 introduced in Equation (14) can be a good aid to satisfy the divergence-free constraint, we plot in Figure 6 the predicted values of $\nabla \cdot \underline{H}$ and the magnitudes of $|\nabla \Phi_2|$ in Figure 7 at the three chosen points $(x = (-0.5, 0, 0.5), y = 0)$ against time. It can be clearly seen from Figure 7 that the values of $\nabla \cdot \underline{H}$ are indeed locally very close to zero, thereby satisfying Gauss' law numerically. The predicted non-zero values of $|\nabla \Phi_2|$ plotted in Figure 8 and the non-zero L_2-norm of $|\nabla \Phi_2|$ plotted in Figure 9 enlighten the necessity of including $\nabla \Phi_2$ in Equation (14) to yield the predicted divergence-free field for $\underline{H}$.

In addition to the good agreement with the exact solution and the satisfaction of the embedded energy conservation in Maxwell's equations, we will also assess the triple-preserving scheme with the well-known Yee's scheme for the sake of completeness. Two schemes will be assessed in terms of the predicted L_2-error norms, rates of convergence, and the required CPU times. To begin with,

DOI: 10.1002/fld

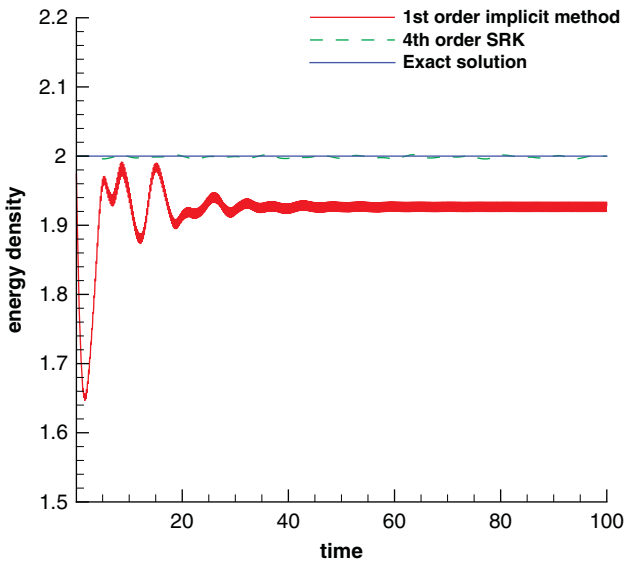

Figure 5. The predicted and exact energy density, shown in (12), against time.

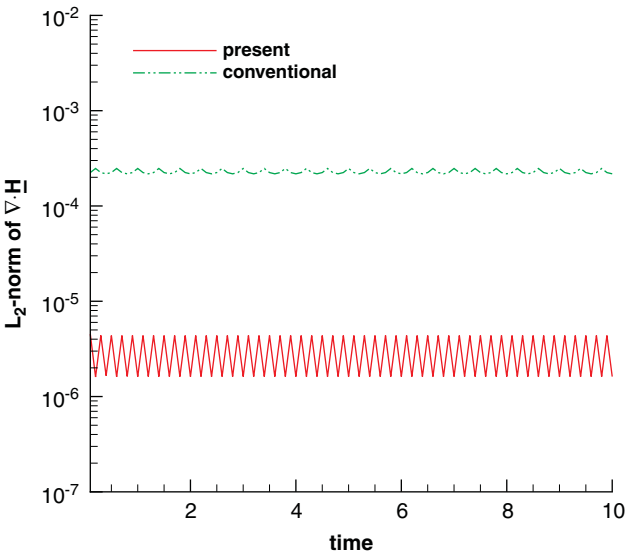

Figure 6. Comparison of the predicted L_2-norms for $\nabla \cdot \underline{H}$ against time using the conventional and the present symplectic formulations.

we plot in Figure 10 the two predicted energy densities against time. One can clearly see from this figure that the predicted energy density of Yee is quickly dropped from two while the energy density predicted by the current triple-preserving scheme remains unchanged with its initial value, which is 2. In addition to this well-preserved nature for W, we also tabulate the predicted L_2-error

DOI: 10.1002/fld

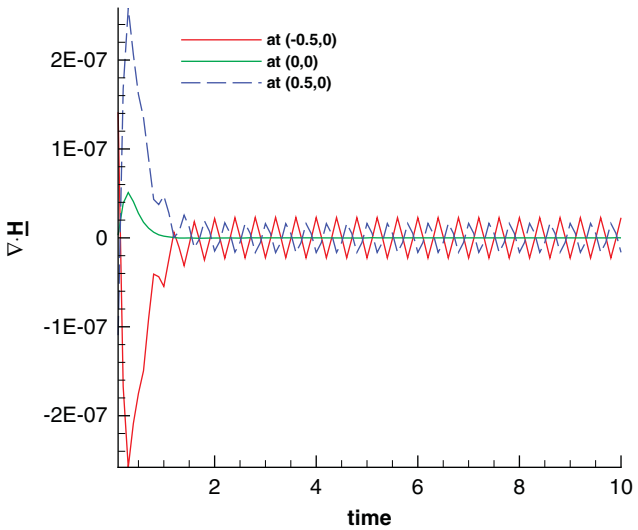

Figure 7. The predicted time-varying values of $\nabla \cdot \underline{H}$ at the three chosen locations.

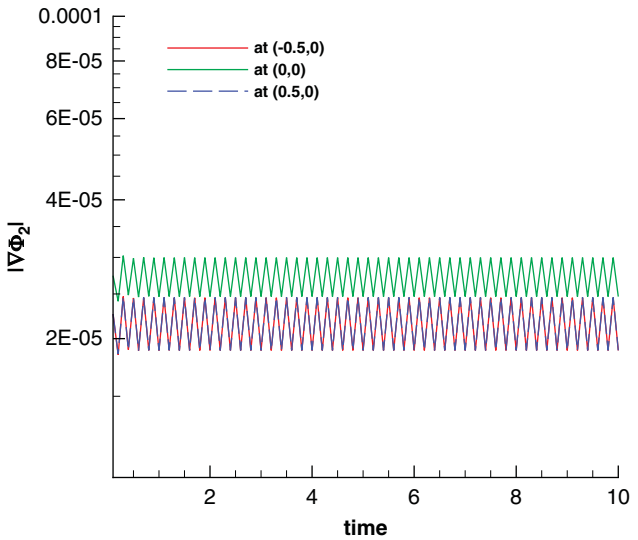

Figure 8. The predicted time-varying values of $|\nabla \Phi_2|$ at the three chosen locations.

norms and the corresponding rates of convergence in Table I. It is clearly shown in this table that the currently proposed preserving scheme outperforms Yee's scheme in providing both higher accuracy and faster convergence rate. While the present scheme needs a much longer computational time to carry out the simulation in each investigated grid, the proposed triple-preserving scheme also outperforms Yee's scheme if comparison is made on the basis of the similar prediction accuracies,

DOI: 10.1002/fld

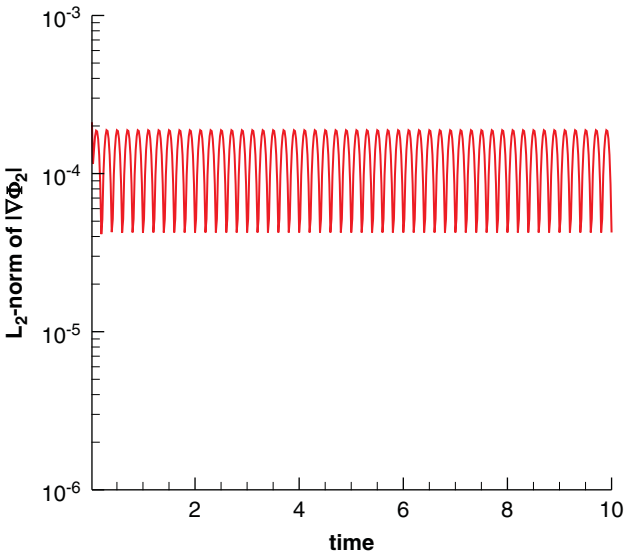

Figure 9. The predicted L_2-norm values of $|\nabla\Phi_2|$ against time.

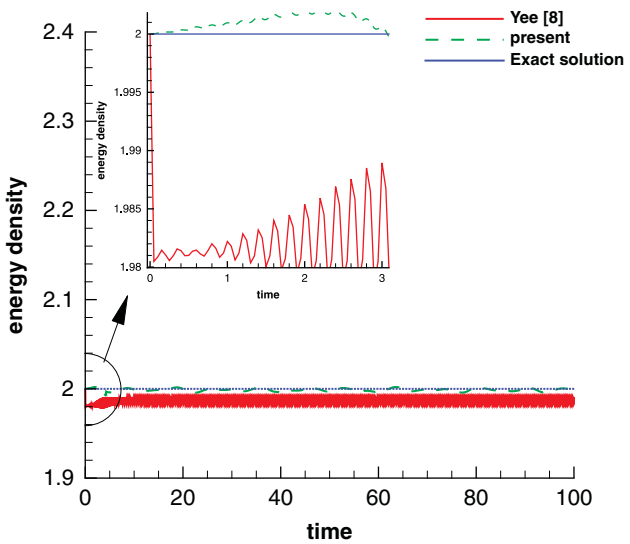

Figure 10. Comparison of the computed energy densities W against time for the problem with the initial value of $W(t=0)=2$.

which are tabulated in Table II. One can clearly see either from Table II or Figure 11 that the present scheme needs less CPU time to accomplish the computation that yields approximately the same level of prediction accuracy.

DOI: 10.1002/fld

Table I. The predicted L_2-error norms, rates of convergence, and the required CPU times for the two investigated schemes carried out in 41^2, 51^2, 61^2, and 71^2 four meshes at time = 10.

	L_2-error norm		Rate of convergence		CPU time (s)	
	Present	Yee [8]	Present	Yee [8]	Present	Yee [8]
41×41	1.5846E−02	0.1478	—	—	6.4375	0.1875
51×51	6.3243E−03	9.2943E−02	4.1163	2.0792	12.5781	0.3594
61×61	3.1331E−03	6.3856E−02	3.8525	2.0587	21.5000	0.6094
71×71	1.7169E−03	4.6592E−02	3.9018	2.0447	33.2187	0.9688

Table II. Comparison of the required CPU times for the two investigated schemes that yield approximately the same L_2-error norms at time = 10.

Present			Yee [8]		
L_2-error norm	Grid	CPU time (s)	L_2-error norm	Grid	CPU time (s)
1.5846E−02	41×41	6.4375	1.5649E−02	121×121	4.6719
6.3243E−03	51×51	12.5781	6.3570E−03	189×189	19.0937
3.1331E−03	61×61	21.5000	3.1511E−03	268×268	56.5937

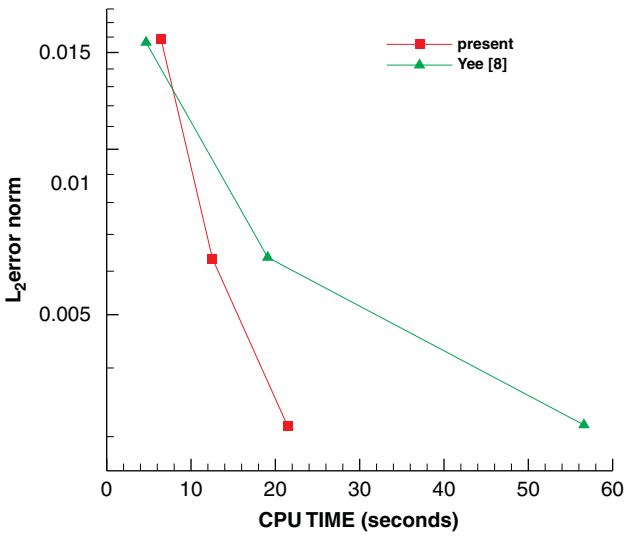

Figure 11. Comparison of the needed CPU times against the predicted L_2-error norms to show that the present scheme needs less CPU time for getting the predicted solution with the same L_2-error norm.

8. CONCLUSIONS

In this article a compact scheme for the first-order derivative terms shown in TM Maxwell's equations has been shown to be applicable to predict the solutions in collocated grids. As a

DOI: 10.1002/fld

good discretization scheme, some features embedded in Maxwell's equations should be retained regardless of the spatial/temporal orders of accuracy. This explains the reasons for employing the symplectic integrator to preserve the Hamiltonian structure. In addition to retain the dispersion relation, the fourth-order accurate divergence-free Maxwell's solutions are also shown to computationally satisfy Gauss' law for magnetism and electricity.

ACKNOWLEDGEMENTS

This work was supported by the National Science Council of the Republic of China under Grants NSC96-2221-E-002-293-MY2, NSC96-2221-E-002-004 and CQSE97R0066-69.

REFERENCES

1. Cockburn B, Li F, Shu CW. Locally divergence-free discontinuous Galerkin methods for the Maxwell equations. *Journal of Computational Physics* 2004; **194**:588–610.
2. Karakashian OA, Jureidini WN. A nonconforming finite element method for the stationary Navier–Stokes equations. *SIAM Journal on Numerical Analysis* 1998; **35**:93–120.
3. Brackbill JU, Barnes DC. The effect of nonzero $\nabla \cdot B$ on numerical solution of the magnetohydrodynamic equations. *Journal of Computational Physics* 1980; **35**:426–430.
4. Evans CR, Hawley JF. Simulation of magnetohydrodynamic flows: a constrained transport method. *Astrophysics Journal* 1998; **332**:659–677.
5. Powell KG. An approximate Riemann solver for magnetohydrodynamics (that works in more than one dimension). *Technical Report*, ICASE, Langley, VA, 1994; 94–95.
6. Torrilhon M. Locally divergence preserving upwind finite volume schemes for magnetohydrodynamic equations, Leona. *SIAM Journal on Scientific Computing* 2005; **26**(4):1166–1191.
7. Rossmanith JA. An unstaggered, high-resolution constrained transport method for magnetohydrodynamic flows. *SIAM Journal on Scientific Computing* 2006; **28**(5):1766–1797.
8. Yee KS. Numerical solution of initial boundary value problems involving Maxwell's equations in isotropic media. *IEEE Transactions on Antenna Propagation* 1996; **AP4**:302–307.
9. Munz CD, Omnes P, Schneider R, Sonnendrücker E, Voβ U. Divergence correction techinques for Maxwell solvers based on a hyperbolic model. *Journal of Computational Physics* 2000; **161**:484–511.
10. Cai JX, Wang YS, Wang B, Jiang B. New multisymplectic self-adjoint scheme and its composition scheme for the time-domain Maxwell's equations. *Journal of Mathematical Physics* 2006; **47**(123508):1–18.
11. Born M, Wolf E. *Principles of Optics*. Pergamon: Oxford, 1964.
12. Jiang BN, Wu J, Povinelli LA. The origin of spurious solutions in computational electromagnetics. *Journal of Computational Physics* 1996; **125**:104–123.
13. Nicolaides RA, Wang DQ. Convergence analysis of a covolume scheme for Maxwell's equations in three dimensions. *Mathematics of Computation* 1998; **67**:947–963.
14. Anderson N, Arthurs AM. Helicity and variational principles for Maxwell's equations. *International Journal of Electronics* 1983; **54**:861–864.
15. Kole JS, Figge MT, De Raedt H. Higher-order unconditionally stable algorithms to solve the time-dependent Maxwell's equations. *Physical Review E* 2002; **65**:0667051–12.
16. Assous F, Degond P, Heintze E, Raviart PA, Serger J. On a finite-element method for solving the three-dimensional Maxwell equations. *Journal of Computational Physics* 1993; **109**:222–237.
17. Morrison PJ. The Maxwell–Vlasov equations as a continuous Hamiltonian system. *Physics Letter* 1980; **80A**: 383–386.
18. Marsden JE, Weinsten A. The Hamiltonian structure of the Maxwell–Vlasov equations. *Physica D* 1982; **4**: 394–406.
19. Lu XW, Schmid R. Symplectic algorithms for Maxwell's equations. *Proceedings of the International Conference on New Applications of Multisymplectic Field Theories*, Salamanca, Spain, 1999; 10–12.
20. Huang ZX, Wu XL. Symplectic partitioned Runge–Kutta scheme for Maxwell's equations. *International Journal of Quantum Chemistry* 2006; **106**:839–842.

DOI: 10.1002/fld

21. Sheu TWH, Lin RK. An incompressible Navier–Stokes model implemented on nonstaggered grids. *Numerical Heat Transfer*, *Part B Fundamentals* 2003; **44**(3):277–294.
22. Chiu PH, Sheu TWH, Lin RK. Development of a dispersion-relation-preserving upwinding scheme for incompressible Navier–Stokes equations on non-staggered grids. *Numerical Heat Transfer*, *Part B Fundamentals* 2005; **48**:543–569.
23. Tam CKW, Webb JC. Dispersion-relation-preserving finite difference schemes for computational acoustics. *Journal of Computational Physics* 1993; **107**:262–281.
24. Chiu PH, Sheu TWH, Lin RK. An effective explicit pressure gradient scheme implemented in the two-level non-staggered grids for incompressible Navier–Stokes equations. *Journal of Computational Physics* 2008; **227**: 4018–4037.
25. Lele SK. Compact finite difference schemes with spectral-like resolution. *Journal of Computational Physics* 1992; **103**:16–42.
26. Bogey C, Bailly C. A family of low dispersive and low dissipative explicit schemes for flow and noise computations. *Journal of Computational Physics* 2004; **194**:194–214.

DOI: 10.1002/fld